

---

# Machine Learning Enabled Brain Segmentation for Small Animal Image Registration

Hendrik Klug<sup>1</sup>

<sup>1</sup>Department of Information Technology and Electrical Engineering, ETH

---

**Abstract** — Cross-subject and cross-study comparability of preclinical imaging data, whole-brain imaging data in particular, is contingent on the quality of registration to a standard reference space. Current methods for neuroimaging rely on full image processing, with high varying intensities outside the brain Region Of Interest that interfere with registration. Applying the processing to a masked image improves the quality of the latter. Here we present a deep learning enabled framework for segmentation of brain tissue in functional and structural MR images that when included in a small animal brain imaging workflow significantly improves the quality of the latter.

## Background

Functional magnetic resonance imaging (fMRI) gives an indirect measurement of brain activity by being sensitive to the change of blood flow. It is one of the most prominent neuroimaging tool for many applications, such as drug discovery and neuromodeling. For these studies, it is imperative that all scans lie in a standard reference frame in order to make meaningful comparisons across the subjects. The common coordinate system enables a statistical evaluation of the likelihood of consistent activation across a group or, in other contexts, the differences in anatomy between two groups. Because of variability both in animal anatomy and in animal preparation, the original MR acquired images are not defined in a common template space. To solve this issue, scans need to be remapped to a reference frame via registration [1, 2]. As reported by Ioanas et al. [3], the legacy approach for mouse-brain image registration is to modify the data in order to conform to pre-existing functions, designed and optimized for human brain imaging. This requires the mouse-data to be adapted to the processing function instead of vice-versa. [3] establishes a novel workflow defined as generic, specifically designed for mouse brain imaging, and benchmarks it against the legacy procedure. While the reported performance increase is considerable, registration is nonetheless influenced by intensity variations outside the brain region. In-vivo as well as ex-vivo MRI head scans, present higher

variability in the viscerocranial and extracranial tissue than in the neurocranium and the brain region of interest. Usage of unmasked (i.e. non brain extracted) data as done by the generic method, can thus lead to stretching or skewing of the brain during the registration process. Computing the transformation solely on the brain volume removes disturbances induced by intensity variations outside the brain region and further improves registration quality.

In recent years it has been shown that convolutional neural networks give the best results for semantic image segmentation in terms of precision and flexibility [4]. Especially the U-Net architecture from Ronneberger et al [5] is to this day one of the most popular in the field of biomedical image segmentation. Training a neural network into a classifier is a supervised method. This means that the model needs to learn its parameters based on observations of labeled data. Manually creating annotations as required to train a deep-learning classifier for high-resolution data is often infeasible, since it requires manual expert segmentation of vast amounts of slices. In the medical domain especially, human labeled data is expensive to acquire and thus very scarce. A much more widely applicable approach is to train the network using the template mask as label together with registered scans. Registration might not be as precise as human labeling, but it is automatic and does not depend on expert input. [6, 7] show that deep learning methods can indeed show satisfiable results when trained with imperfect training data. While our purpose was to create a workflow that generates better masks than the one from the template space, we show that the latter can be used as training data for the deep-learning model, by applying small changes to it.

In this study we investigate whether and in how far reliable classification can be obtained from imperfect training data and whether preclinical image masking improves an optimized registration workflow. We also integrate the question of reusability and reproducibility. This is done in a fully open and reproducible fashion and the resulting applicable program is distributed as FOSS.

We evaluate the effects of our classifier on a full-fledged registration workflow via the benchmarking

algorithms from [3].

## Classifier Implementation

We lay out a preparatory step to improve brain registration by specifically extracting the brain volume from the MRI scans. Our solution utilises a machine learning enabled brain tissue classifier, and the software implementation is formulated to integrate with the SAMRI Generic workflow [3], in order to ensure broader usability and reproducible benchmarking. It creates a mask of the brain region using a classifier, which is then used to extract the region of interest. Two classifiers were trained, one for scans acquired with RARE sequences yielding  $T_2$ -weighted contrast and one scans acquired with gradient-echo EPI sequences yielding either BOLD [8] and CBV [9] contrasts section 5.2. The brain extraction nodes of the workflow return both the masked input and the binary mask. The latter is used to constrain image similarity metric estimation on the relevant region of interest (ROI), while the extracted brain volume is used to prevent drifting of extracranial hyperintensities into the ROI. The registration transformation is applied to the unmasked data to make the process minimally destructive.

The assignment of “brain” and “not brain” annotation to each voxel in the scans is performed via a trained U-Net, a popular neural network for medical image segmentation.

## Training Data

To improve general-purpose application, training examples need to be drawn from a usually unknown probability distribution, which is expected to be representative of the space of occurrences. We set up an occurrence space from which the data of interest is drawn, consisting of all the different mouse brain MRI data sets coming from multiple experiments, with their corresponding labels. Based on an approximation of the occurrence space, the network builds a general model that enables it to extrapolate and produce sufficiently accurate predictions in new cases.

As a training dataset, we use scans which were pre-processed with the SAMRI Generic workflow. This data thus contains scans mapped onto a bregma-centered standard [3] space derived from the Toronto Hospital for Sick Children Mouse Imaging Center brain template [10]. A template-based mask is available in the same reference space, and constitutes a ground truth estimation. As registration in the absence of brain extraction is prone to imperfections, the mask does not always align perfectly with the brain region of every slice and some scans had to be removed manually.

## Evaluation

For the quality control of the workflow, we first evaluate the classification process, followed by a benchmark between the Generic and the improved (Masked) workflow.

### Classification

Quality control of our classifier is difficult in the sense that it should predict a better mask than the template. Nevertheless, it is useful to verify whether the output is similar, as it should be. As a similarity metric between the template mask and the classifier output we have used the Dice score (see eq. (1)). The average Dice score taken on every slice of the test data set is  $D_{coef} = 0.931 \sim 1$ , indicating that classifier output has only minor changes in comparison with the template.

### Workflow

We use an established palette of workflow evaluation metrics — inspecting volume and smoothness conservation, as well as downstream effects on basic functional analysis [3] — to benchmark the novel SAMRI Masked workflow against the SAMRI Generic workflow. In order to provide a statistical evaluation of the quality of registration, we evaluate a bootstrapped distribution of the respective root mean squared error (RMSE) to the optimal value of 1 for volume conservation and smoothness conservation.

### Volume Conservation

Volume Conservation Factor (VCF) [3] measures the registration induced deformation of the scanned brain, by computing the ratio of the brain volume before and after preprocessing. A positive ratio indicates that the brain was stretched to fill the template space, while a negative ratio indicates that non-brain voxels were introduced in the template brain space. Volume conservation is highest for a VCF equal to 1, indicating that the preprocessing has no influence on the brain volume of the scans.

As seen in fig. 2a, we note that in the described dataset VCF is sensitive to the workflow ( $F_{1,132} = 0.024, p = 0.88$ ), but not the interaction of the workflow with the contrast ( $F_{1,132} = 0.1, p = 0.75$ ). The performance of the Generic SAMRI workflow is different from that of Generic\*, yielding a two-tailed p-value of 0.64. With respect to the data break-up by contrast (CBV versus BOLD, fig. 2a), we see no notable main effect for the contrast variable (VCF of  $-0.03$ , 95%CI:  $-0.05$  to  $0.00$ ), nor do we report a notable effect for the contrast-workflow interaction (VCF of  $-0.01$ , 95%CI:  $-0.02$  to  $0.01$ ).

We note that there is a significant variance decrease in all conditions for the Masked workflow (0.32-fold). Further, we note that the root mean squared error ratio favours the Masked workflow ( $\text{RMSE}_{G^*}/\text{RMSE}_G \simeq 0.75$ ). Evaluating a boot-

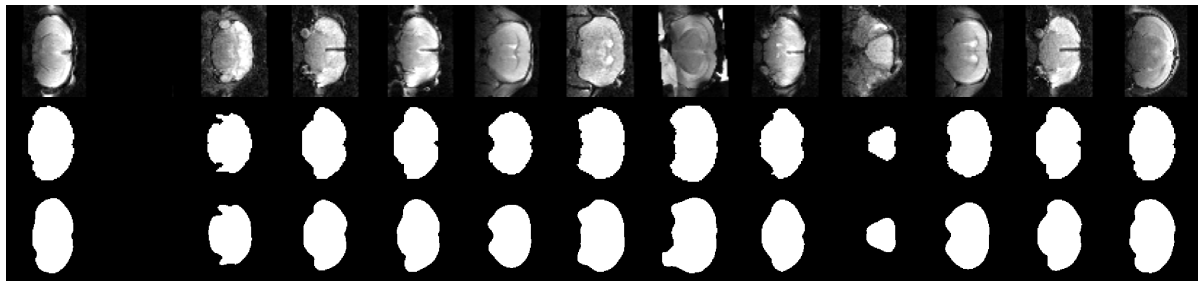


**Figure 1: The Classifier predicts a similar mask to the ground truth.** Randomly picked plots from the test set illustrate the predictions of the classifier. The first row presents the input image, the second the ground truth and the third row shows the predictions of the classifier.

strapped distribution of the respective Root Mean Squared Errors (RMSE) to the optimal VCF 1, we report that it is sensitive to the workflow (RMSE of  $-0.02$ , 95%CI:  $-0.02$  to  $-0.02$ ) and the contrast-workflow interaction (RMSE of  $0.01$ , 95%CI:  $0.01$  to  $0.01$ ).

### Smoothness Conservation

Smoothing is a popular tool employed by many pre-processing functions to increase the signal-to-noise ratio. Image smoothness comes at the cost of image contrast as well as feature saliency and has been shown to result in inferior anatomical alignment [11] due to the loss of spatial resolution. As an indicator of image smoothness induced by the workflow, the Smoothness Conservation Factor (SCF) [3] expresses the ratio between the smoothness of the preprocessed images and the smoothness of the original images. Smoothness Conservation is highest for a SCF equal to 1, indicating that the preprocessing does not influence image smoothness.

While the performance of the Generic SAMRI workflow is only slightly different from that of the Masked workflow, the root mean squared error ratio favors the Masked workflow ( $\text{RMSE}_{G^*}/\text{RMSE}_G \approx 1.1$ ).

Descriptively, we observe that neither the Generic nor the Masked workflow introduce a strong smoothing (SCF of  $-0.01$ , 95%CI:  $-0.02$  to  $0.01$ ).

Further, we note that there is a notable variance decrease for the Masked workflow (1.16-fold).

Given the break-up by contrast shown in fig. 2b, we see no effect for the contrast variable (SCF of  $0.06$ , 95%CI:  $0.03$  to  $0.09$ ) and the contrast-workflow interaction (SCF of  $0.01$ , 95%CI:  $-0.01$  to  $0.03$ ).

Evaluating a bootstrapped distribution of the respective Root Mean Squared Errors (RMSE) to 1, we report that the RMSE is sensitive to the workflow (RMSE of  $-0.02$ , 95%CI:  $-0.02$  to  $-0.02$ ) and the contrast-workflow interaction (RMSE of  $0.01$ , 95%CI:  $0.01$  to  $0.01$ ).

### Functional Analysis

Functional Analysis expresses the significance detected across all voxels of a scan by computing the Mean Significance (MS) [3].

We observe that the Masked level of the workflow variable does not introduce a notable significance loss (MS of  $-0.04$ , 95%CI:  $-0.07$  to  $-0.01$ ). Furthermore, we note a slight variance decrease in all conditions for the Masked workflow (0.92-fold).

With respect to the data break-up by contrast (fig. S1), we see no notable main effect for the contrast variable (MS of  $-0.09$ , 95%CI:  $-0.87$  to  $0.68$ ).

### Variance Analysis

As an additional metric for the comparison between workflows, we evaluate if physiological meaningful variability is retained across repeated measurements. It is based on the assumption that adult mouse brains retain size, shape, and implant position in the absence of intervention, throughout the 8 week study period [3]. Examining the similarity between the template and preprocessed scans, session-wise variability should be smaller than subject-wise variability. This comparison is performed using a type 3 ANOVA, modeling both the subject and the session variables. For this assessment three metrics are used, with maximal sensitivity to different features: Neighborhood Cross Correlation (CC, sensitive to localized correlation), Global Correlation (GC, sensitive to whole-image correlation), and Mutual Information (MI, sensitive to whole-image information similarity).

Figure 3 renders the similarity metric scores for both the SAMRI Generic and Masked workflows. Both, the Generic and the Masked workflow produce results which show a higher F-statistic for the subject than for the session variable. For the Masked workflow, F-statistics show: CC (subject:  $F_{10,19} = 11.48$ ,  $p = 4.34 \times 10^{-6}$ , session:  $F_{4,19} = 4.115$ ,  $p = 0.014$ ), GC (subject:  $F_{10,19} = 4.162$ ,  $p = 0.0037$ , session:  $F_{4,19} = 2.077$ ,  $p = 0.12$ ), and MI (subject:  $F_{10,19} = 2.348$ ,  $p = 0.053$ , session:  $F_{4,19} = 2.092$ ,  $p = 0.053$ ).

0.12).

For the Generic SAMRI workflow, resulting data F-statistics show: CC (subject:  $F_{10,19} = 4.472$ ,  $p = 0.0025$ , session:  $F_{4,19} = 1.969$ ,  $p = 0.14$ ), GC (subject:  $F_{10,19} = 2.04$ ,  $p = 0.087$ , session:  $F_{4,19} = 1.035$ ,  $p = 0.41$ ), and MI (subject:  $F_{10,19} = 0.97$ ,  $p = 0.5$ , session:  $F_{4,19} = 1.805$ ,  $p = 0.17$ ).

## Discussion

The classifier improves the volume conservation, smoothness conservation, and session-to-session consistency of the SAMRI Generic workflow in terms of precision while conserving accuracy.

Region assignment validity is also revealed in a qualitative examination of higher-level functional maps (fig. S2), where both the Generic and the Generic Masked workflow provide accurate coverage of the sampled volume for both BOLD and CBV fMRI data.

These benefits of the classifier are robust to the functional contrast (figs. 2a and 2b), with the Generic Masking workflow being less or equally susceptible to the contrast variable, when compared to the Generic workflow.

The classifier improves the performance of the SAMRI Generic workflow, making these accessible in the same interface with the same advantages in terms of transparency, parametrization, ease of package management, and non-destructive metadata management. The complete workflow of this report is fully reproducible and thus easily verifiable. We make public the functions used for the masking in the workflow as well as those used to train the classifier, through the *mlebe* [12] python package.

Our workflow has the advantage that the performance of a Neural Network can increase when trained further with new data. The FOSS distribution model for both the classifier and workflow, as well as the article, allows users to easily take advantage of the classifier extendability and recreate the steps described herein. Registering new data with the Generic Maksed workflow can increase the size of the training data set of the classifier. After removing possibly bad registrations, the latter can be trained again, which will improve its generalisation capability. Another advantage of the trainability of the classifier and the openly published code is that this workflow can be adapted to a wast variety of data types.

## Conclusion

We present a remodeled version of the SAMRI Genetic registration workflow, which offers several advantages summarized by established metrics for data features commonly biased by registration. Comparison with the original SAMRI Generic workflow revealed superior performance of the SAMRI Generic Masked workflow in terms of volume and smoothness

conservation, as well as variance structure across subjects and sessions. The easily accessible, optimized registration parameters of the SAMRI Generic Workflow as well as the open source code to the classifier training functions make the pipeline transferable to any other imaging applications. The open source software choices in both the workflow and this article's source code empower users to better verify, understand, remix, and reuse our work.

## Methods

For the benchmarking of the two workflows, the same methods that are described in the original paper have been applied in this work. A more detailed description can be found there.

### Model

As the architecture of the classifier, the U-Net from Ronneberger et al [5] was chosen based on its high performance in the field of biomedical image segmentation. This is a convolutional neural network that consists of a contracting path that captures context in addition to a symmetric expanding path that enables precise localization. Localization in this context means that a class label is assigned to each pixel. We used the U-Net implementation from zhixuhao [13], written in Keras. Keras is a high-level neural networks API, written in Python and capable of running on top of TensorFlow, CNTK, or Theano. It allows for easily readable code and thus makes the workflow easier to reproduce.

The implementation of the U-Net from zhixuhao has, in addition to the original architecture, two drop-out layers. A drop-out layer randomly sets a fraction of input units from the layer to 0 at each update during training time. The set fraction rate is 0.5. It is known that dropout helps prevent overfitting and greatly improves the performance of deep learning models [14].

The model was trained using the Dice loss, which is computed from the Dice score. It calculates the similarity of two binary samples X and Y with

$$D_{coef} = \frac{2|X \cap Y|}{|X| + |Y|} \quad (1)$$

It is a quantity ranging from 0 to 1 that is to be maximized. The loss is then calculated with  $1 - D_{coef}$ . Because the Dice loss is not differentiable, small changes need to be made. In our case, the two samples to be compared are normalized, grey valued images and are thus not binary but have values between 0 and 1. Additionally, instead of using the logical operation *and*, element wise products are used to approximate the non-differentiable intersection operation. To avoid a division by zero, +1 is added on the numerator and denominator.

Because many more pixels in the masks are 0 than 1, there is a class imbalance problem. This is a prob-

lem because in this case a false positive gives a much higher loss than a false negative. For example, predicting only black would give an acceptable loss, while predicting only white pixels would not. Using the Dice coefficient as a loss function for training should make it invariant to this class imbalance problem as stated by Fausto Milletari et al. in [15].

## Data Set

The data set consists of 3D MR images taken from an aggregation of three studies: irsabi [16], opfvta [17], drlfom [18] and other unpublished data, acquired with similar parameters.

The measured animals were fitted with an optic fiber implant ( $l = 3.2 \text{ mm}$   $d = 400 \mu\text{m}$ ) targeting the Dorsal Raphe (DR) nucleus in the brain stem. Using this dataset shows that the classifier is robust to these types of experiment setups.

Images from the irsabi study are only used for quality control of the registration and are thus unknown to the classifier. It is the same dataset that was used to benchmark the Generic workflow in the original paper and thus allows for a better estimation of the general performance of our improved pipeline.

The images are transformed into a standard space using a template mask via SAMRI [19] and are thus defined in the same affine space. SAMRI is a data analysis package of the ETH/UZH Institute for Biomedical Engineering. It is equipped with an optimized registration workflow and standard geometric space for small animal brain imaging [3].

Because of variance in mouse brain anatomy and in the experiment setup, some of the transformed data do not overlap perfectly with the reference template. To filter these images out, most of the incongruent slices were removed manually from the data set.

For the registration of the images, a padding was needed to make the originally not affine space affine. As a result, the 3D volumes present many zero-valued slices, some of them overlapping with the mask.

Since it is not wanted for the model to predict a mask on black slices, the mask is set to zero where the image is zero-valued. Because some pixels representing the brain tissue are zero-valued, holes result from this operation. To patch these, the function `binary_fill_holes` from `scipy.ndimage.morphology` [20] is used. An example of the preprocessing can be seen in fig. 4.

In the coronal view, each slice of the transformed data is originally of shape  $(63, 48)$ , matching the reference space resolution of  $200 \mu\text{m}$ . It is then reshaped into  $(128, 128)$  by first zero-padding the smaller dimension to the same size as the bigger one and then reshaping the image into  $128$  using the function `cv2.resize` from the opencv python package [21].

Finally, the images are normalized by first clipping them from the minimum to the 99th percentile of the data to remove outliers and then divided by the maximum.

The data set is separated into Training, Validation and Test sets such that 90% of the total data are used for training and validation while 10% are used for testing. This is done with the help of the function `train_test_split` from the package `sklearn.model_selection` [22]. The Validation set is used for the optimization of hyperparameters while the Test set is used as a measure of extrapolation capability.

## Data Augmentation

Because of diverse settings in the experiment setup, including animal manipulations causing artifacts, MR image quality can differ substantially between labs and even individual study populations. To account for these variations, we apply an extensive set of transformations to our data. This includes rotations of up to  $90^\circ$ , a width and height shift range of 30 pixels, a shear range of 0.5 pixels, zoom range of 0.3, brightness range of  $(0.7, 1.3)$  and horizontal as well as vertical flips. Additionally a gaussian noise with a variance range of  $(0, 0.001)$  is added to the image.

This not only increases the data set size but also makes it more representative of the general data distribution of mice brain MR images and results in a model with a better generalization capability.

Many more sophisticated methods have been tested, but it has been shown that one of the more successful data augmentation strategies is the simple transformations mentioned above [23].

## Training

The model was trained slice wise, with the coronal view and 600 as the maximum number of epochs. The coronal view was chosen over the axial one, because the shapes of the masks are much simpler in the coronal view and thus easier to learn for the network.

Additionally, the coronal view has the advantage of higher resolution as the MR images were recorded coronally.

To improve the learning process of the network, two callbacks from Keras were used [24]. "`ReduceLROnPlateau`" reduces the learning rate when the validation loss has stopped improving and "`EarlyStopping`" stops the training when the validation loss has stopped improving for a number of epochs. The latter reduces computation time and prevents overfitting.

## Masking

To improve the SAMRI registration workflow, an additional node is implemented where the images are masked, such that only the brain region remains. To alleviate the task of the classifier, the image is first bias-corrected using the "`N4BiasFieldCorrection`" function of the ANTs package, with spatial parameters used in the samri functions. The image is then resampled into the resolution of the template space, which has a voxel size of  $0.2 \times 0.2 \times 0.2$ . This is done

with the *Resample* command from the FSL library which is an analysis tool for FMRI, MRI and DTI brain imaging data [25]. Then, the image is preprocessed using the operations described in section 5.2. Since the classifier was trained to predict on images of shape (128, 128), the input needs to be reshaped. The slice-wise predictions of the model are reconstructed to a 3D mask via the command *NiftiImage* from the neuroimaging python package nibabel [26]. This is done using the same affine space as the input image. The latter is then reshaped into the original shape inverting the preprocessing step, either with the opencv resize method or by cropping. Additionally, the binary mask is resampled into its original affine space, before being multiplied with the brain image to extract the ROI. The workflow then continues with only the Region Of Interest as the image.

## Metrics

The VCF uses the 66<sup>th</sup> voxel intensity percentile of the raw scan before any processing as definition of the brain volume. The VCF is then obtained with eq. (2), where  $v$  is the voxel volume in the original space,  $v'$  the voxel volume in the transformed space,  $n$  the number of voxels in the original space,  $m$  the number of voxels in the transformed space,  $s$  a voxel value sampled from the vector  $S$  containing all values in the original data, and  $s'$  a voxel value sampled from the transformed data.

$$VCF = \frac{v' \sum_{i=1}^m [s'_i \geq P_{66}(S)]}{v \sum_{i=1}^n [s_i \geq P_{66}(S)]} = \frac{v' \sum_{i=1}^m [s'_i \geq P_{66}(S)]}{v[0.66n]} \quad (2)$$

The bootstrapped distribution of the RMSE (eq. (3)) is obtained by resampling the VCF distributions 10000 times with replacement, and computing the RMSE for every sample.

$$RMSE = \sqrt{\text{mean}((1 - VCF)^2)} \quad (3)$$

The SCF metric is based on the ratio of smoothness before and after processing. It is obtained via eq. (4), where  $r$  is the distance of two amplitude distribution samples,  $a$  is the relative weight of the Gaussian term in the model,  $b$  is the width of the Gaussian and  $c$  the decay of the mono-exponential term [27].

$$ACF(r) = a * e^{-r^2/(2*b^2)} + (1 - a) + e^{-r/c} \quad (4)$$

The for the MS relevant statistical power is obtained via the negative logarithm of first-level p-value maps. Voxelwise statistical estimates for the probability that a time course could — by chance alone — be at least as well correlated with the stimulation regressor as the voxel time course measured are averaged via eq. (5), where  $n$  represents the number of statistical estimates in the scan, and  $p$  is a p-value.

$$MS = \frac{\sum_{i=1}^n -\log(p_i)}{n} \quad (5)$$

## Data and Code Availability

The data archive relevant for this article is freely available [?], and automatically accessible via the Gentoo Linux package manager. In addition to the workflow code [12, 28], we openly release the re-executable source code [29] for all statistics and figures in this document. The herein introduced novel method as well as the benchmarking are thus fully transparent and reusable for further data.

## References

- [1] J B Antoine Maintz and Max A Viergever. An Overview of Medical Image Registration Methods. page 22.
- [2] Aristeidis Sotiras, Christos Davatzikos, and Nikos Paragios. Deformable Medical Image Registration: A Survey. *IEEE Transactions on Medical Imaging*, 32(7):1153–1190, July 2013. ISSN 1558-254X. doi: 10.1109/TMI.2013.2265603.
- [3] Horea-Ioan Ioanăs, Markus Marks, Mehmet Fatih Yanik, and Markus Rudin. An Optimized Registration Workflow and Standard Geometric Space for Small Animal Brain Imaging. preprint, Neuroscience, April 2019. URL <http://biorxiv.org/lookup/doi/10.1101/619650>.
- [4] Qichuan Geng, Zhong Zhou, and Xiaochun Cao. Survey of recent progress in semantic image segmentation with CNNs. *Science China Information Sciences*, 61(5):051101, May 2018. ISSN 1674-733X, 1869-1919. doi: 10.1007/s11432-017-9189-6. URL <http://link.springer.com/10.1007/s11432-017-9189-6>.
- [5] Olaf Ronneberger, Philipp Fischer, and Thomas Brox. U-Net: Convolutional Networks for Biomedical Image Segmentation. *arXiv:1505.04597 [cs]*, May 2015. URL <http://arxiv.org/abs/1505.04597>. arXiv: 1505.04597 version: 1.
- [6] Nima Tajbakhsh, Laura Jeyaseelan, Qian Li, Jeffrey N. Chiang, Zhihao Wu, and Xiaowei Ding. Embracing imperfect datasets: A review of deep learning solutions for medical image segmentation. page 101693. ISSN 1361-8415. doi: 10.1016/j.media.2020.101693. URL <http://www.sciencedirect.com/science/article/pii/S136184152030058X>.
- [7] Imperfect segmentation labels: How much do they matter? URL [https://www.researchgate.net/publication/325733789 Imperfect\\_Segmentation\\_Labels\\_How\\_Much\\_Do\\_They\\_Matter](https://www.researchgate.net/publication/325733789 Imperfect_Segmentation_Labels_How_Much_Do_They_Matter). Library Catalog: www.researchgate.net.

- [8] Seiji Ogawa, Tso-Ming Lee, Asha S. Nayak, and Paul Glynn. Oxygenation-sensitive contrast in magnetic resonance image of rodent brain at high magnetic fields. *Magnetic Resonance in Medicine*, 14(1):68–78, April 1990. doi: 10.1002/mrm.1910140108. URL <https://doi.org/10.1002/mrm.1910140108>.
- [9] John J.A. Marota, C. Ayata, Michael A. Moskowitz, Robert M. Weisskoff, Bruce R. Rosen, and Joseph B. Mandeville. Investigation of the early response to rat forepaw stimulation. *Magnetic Resonance in Medicine*, 41(2):247–252, February 1999. doi: 10.1002/(sici)1522-2594(199902)41:2<247::aid-mrm6>3.0.co;2-u. URL [https://doi.org/10.1002/\(sici\)1522-2594\(199902\)41:2<247::aid-mrm6>3.0.co;2-u](https://doi.org/10.1002/(sici)1522-2594(199902)41:2<247::aid-mrm6>3.0.co;2-u).
- [10] A.E. Dorr, J.P. Lerch, S. Spring, N. Kaban, and R.M. Henkelman. High resolution three-dimensional brain atlas using an average magnetic resonance image of 40 adult c57bl/6j mice. *NeuroImage*, 42(1):60–69, August 2008. doi: 10.1016/j.neuroimage.2008.03.037. URL <https://doi.org/10.1016/j.neuroimage.2008.03.037>.
- [11] Oscar Esteban, Christopher Markiewicz, Ross W Blair, Craig Moodie, Ayse Ilkay Isik, Asier Erramuzpe Aliaga, James Kent, Mathias Goncalves, Elizabeth DuPre, Madeleine Snyder, et al. FMRIprep: a robust preprocessing pipeline for functional MRI. *Nature Methods*, page 111–116, December 2019. doi: 10.1038/s41592-018-0235-4. URL <https://doi.org/10.1038/s41592-018-0235-4>.
- [12] Hendrik\\_Klug. Jimmy2027/MLEBE, . URL <https://github.com/Jimmy2027/MLEBE>. original-date: 2019-10-13T09:57:20Z.
- [13] zhixuhao. zhixuhao/unet, January 2020. URL <https://github.com/zhixuhao/unet>. original-date: 2017-04-06T01:58:15Z.
- [14] Nitish Srivastava, Geoffrey Hinton, Alex Krizhevsky, Ilya Sutskever, and Ruslan Salakhutdinov. Dropout: a simple way to prevent neural networks from overfitting. *The journal of machine learning research*, 15(1):1929–1958, 2014.
- [15] Fausto Milletari, Nassir Navab, and Seyed-Ahmad Ahmadi. V-Net: Fully Convolutional Neural Networks for Volumetric Medical Image Segmentation. *arXiv:1606.04797 [cs]*, June 2016. URL <http://arxiv.org/abs/1606.04797>. arXiv: 1606.04797.
- [16] Horea-Ioan Ioanas and Markus Rudin. BIDS Data for "An Optimized Registration Workflow and Standard Geometric Space for Small Animal Brain Imaging", April 2019. URL <https://doi.org/10.5281/zenodo.2651640>.
- [17] Horea-Ioan Ioanas, Bechara John Saab, and Markus Rudin. A Whole-Brain Map and Assay Parameter Analysis of Mouse VTA Dopaminergic Activation. page 19, .
- [18] Horea-Ioan Ioanas, Bechara John Saab, and Markus Rudin. Effects of Acute and Chronic Reuptake Inhibition on Optogenetically Induced Serotonergic Activity. page 20, .
- [19] IBT-FMI/SAMRI, December 2019. URL <https://github.com/IBT-FMI/SAMRI>. original-date: 2015-04-27T00:26:08Z.
- [20] Multi-dimensional image processing (scipy.ndimage) — SciPy v1.4.1 Reference Guide, . URL <https://docs.scipy.org/doc/scipy/reference/ndimage.html#morphology>.
- [21] opencv-python: Wrapper package for OpenCV python bindings., . URL <https://github.com/skvark/opencv-python>.
- [22] F. Pedregosa, G. Varoquaux, A. Gramfort, V. Michel, B. Thirion, O. Grisel, M. Blondel, P. Prettenhofer, R. Weiss, V. Dubourg, J. Vanderplas, A. Passos, D. Cournapeau, M. Brucher, M. Perrot, and E. Duchesnay. Scikit-learn: Machine learning in Python. *Journal of Machine Learning Research*, 12:2825–2830, 2011.
- [23] Luis Perez and Jason Wang. The Effectiveness of Data Augmentation in Image Classification using Deep Learning. *arXiv:1712.04621 [cs]*, December 2017. URL <http://arxiv.org/abs/1712.04621>. arXiv: 1712.04621.
- [24] Callbacks - Keras Documentation, . URL <https://keras.io/callbacks/>.
- [25] Mark Jenkinson, Christian F Beckmann, Timothy EJ Behrens, Mark W Woolrich, and Stephen M Smith. Fsl. *Neuroimage*, 62(2):782–790, 2012.
- [26] Neuroimaging in Python — NiBabel 2.5.0 documentation, . URL <https://nipy.org/nibabel/>.
- [27] Robert W Cox, Gang Chen, Daniel R Glen, Richard C Reynolds, and Paul A Taylor. FMRI clustering in AFNI: false-positive rates redux. *Brain connectivity*, 7(3):152–171, April 2017. doi: 10.1089/brain.2016.0475. URL <https://doi.org/10.1089/brain.2016.0475>.
- [28] Horea-Ioan Ioanas, Markus Marks, Dominik Schmidt, Florian Aymanns, and Markus Rudin. SAMRI — Small Animal Magnetic Resonance

Imaging, November 2017. URL <https://doi.org/10.5281/zenodo.1044033>.

- [29] Hendrik\\_Klug. Jimmy2027/mlebe\_repsep, .  
URL [https://github.com/Jimmy2027/mlebe\\_RepSep](https://github.com/Jimmy2027/mlebe_RepSep). original-date: 2020-01-20T16:51:45Z.

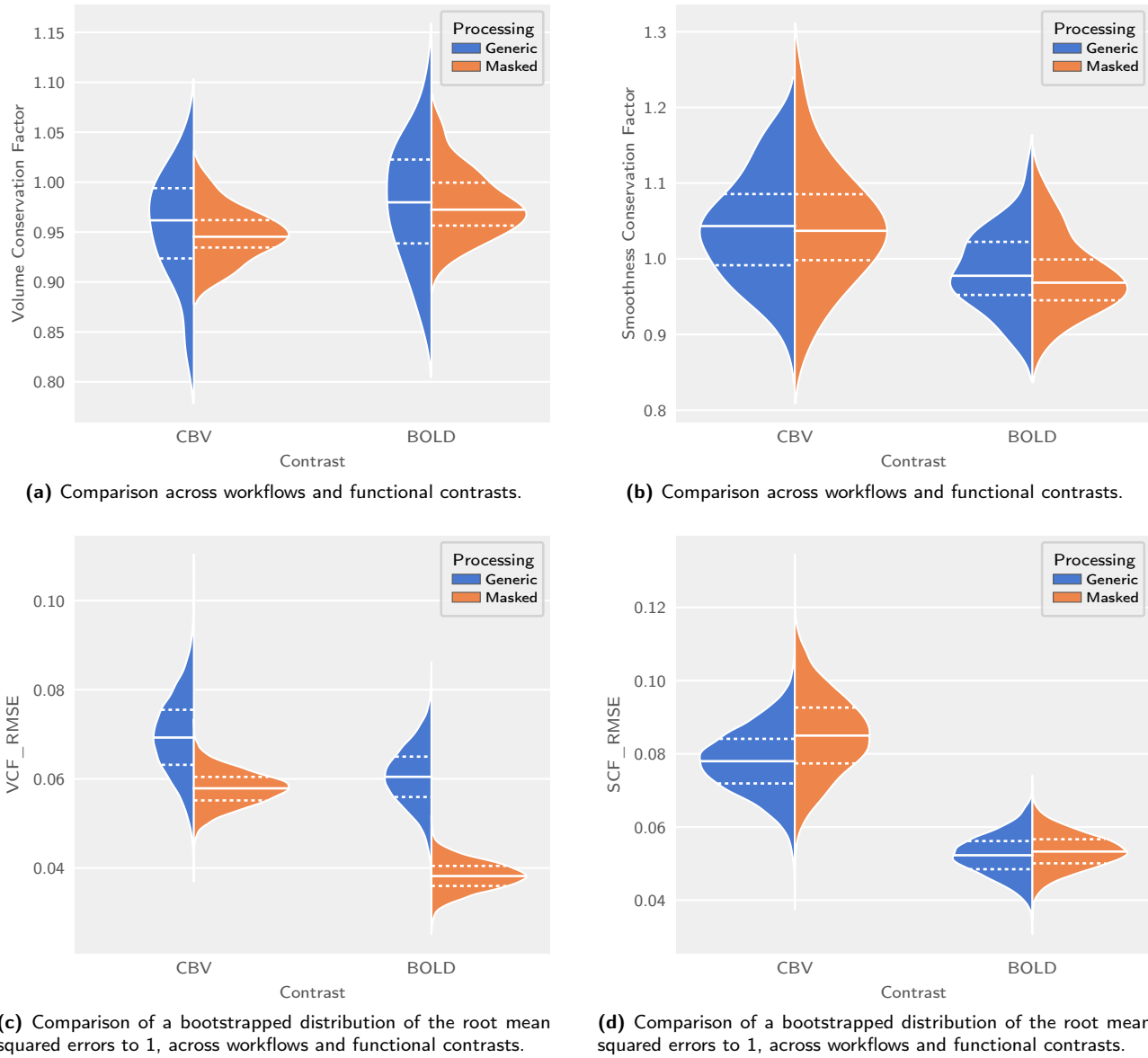


**Figure 2: Both the SAMRI Generic and the Masked workflow optimally and reliably conserve volume and smoothness, the latter showing values that are closely distributed to 1. Plots showing the distribution of two target metrics in the first row, together with the respective bootstrapped distributions of the RMSEs in the second row. Solid lines in the colored distribution densities indicate the sample mean and dashed lines the inner quartiles.**

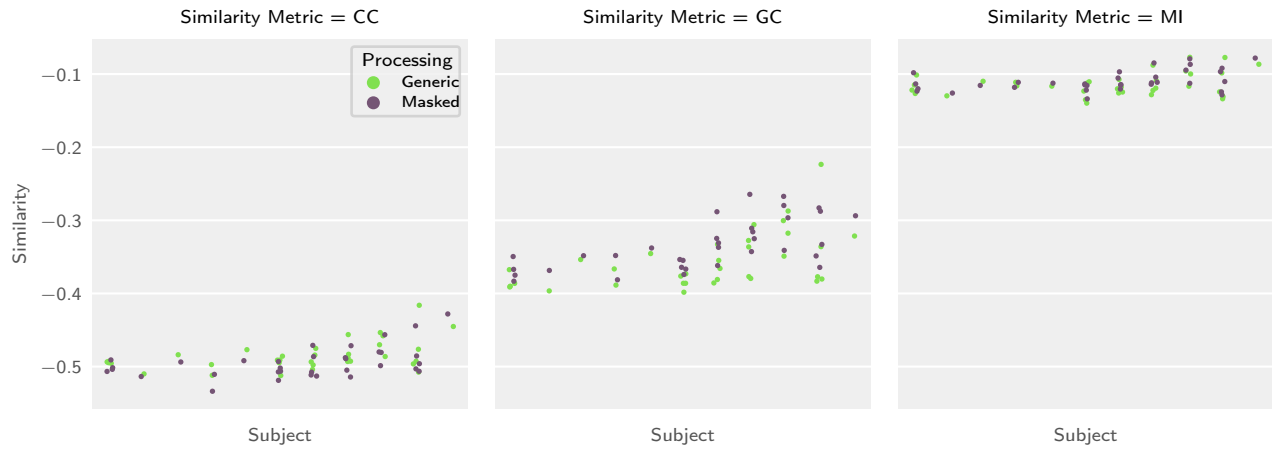
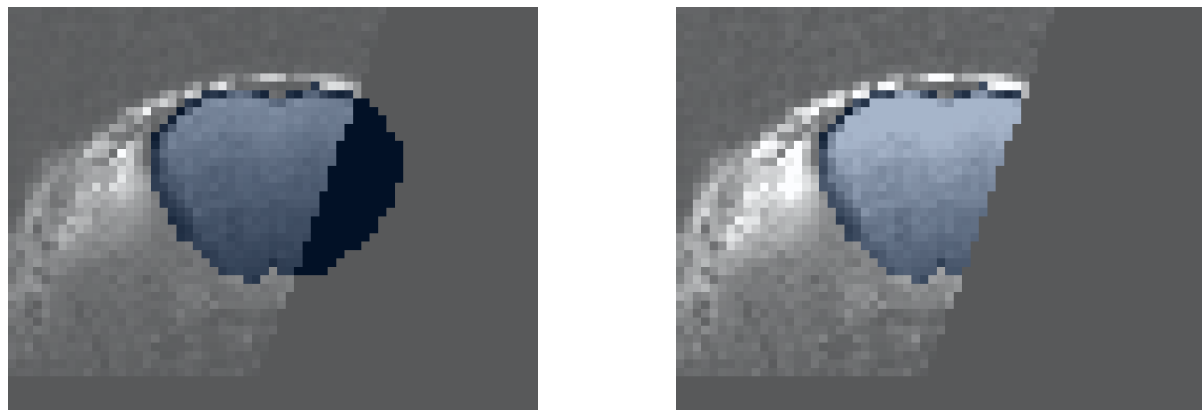


**Figure 3: Both the Generic and the Masked workflow minimize trial-to-trial variability while conserving subject-wise variability.** Swarmplots of three metric scores illustrate similarity of preprocessed images for the two corresponding workflow templates, plotted across subjects (separated into x-axis bins) and sessions (individual points in each x-axis bin), for the CBV contrast.



(a) Example of an unpreprocessed slice.

(b) Example of a preprocessed slice.

**Figure 4: The preprocessing removes the mask there, where the image-pixelvalues are 0.** Plots of the same image, superposed with the template mask, with and without preprocessing.

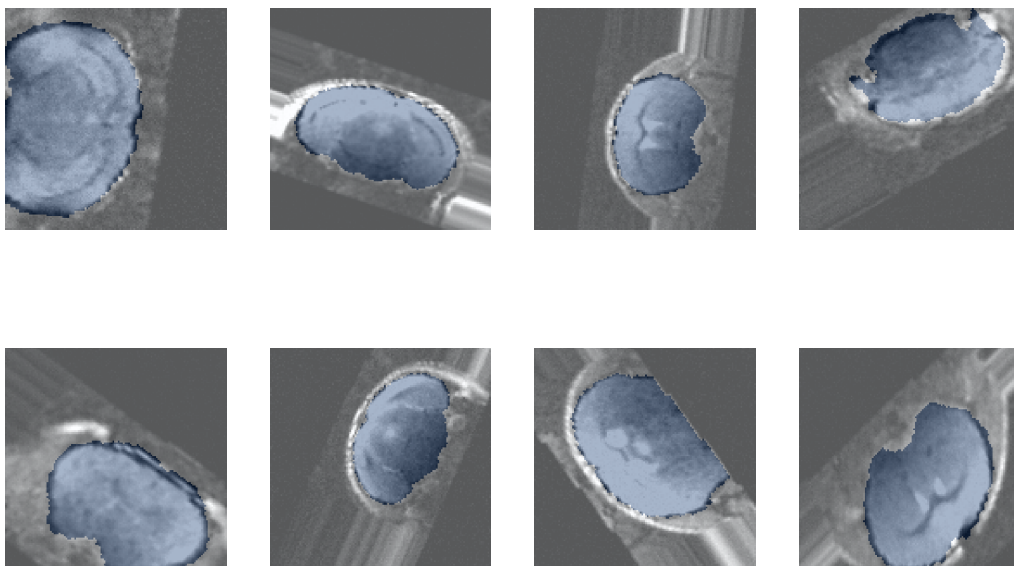


**Figure 5:** Augmented samples from the Training set.

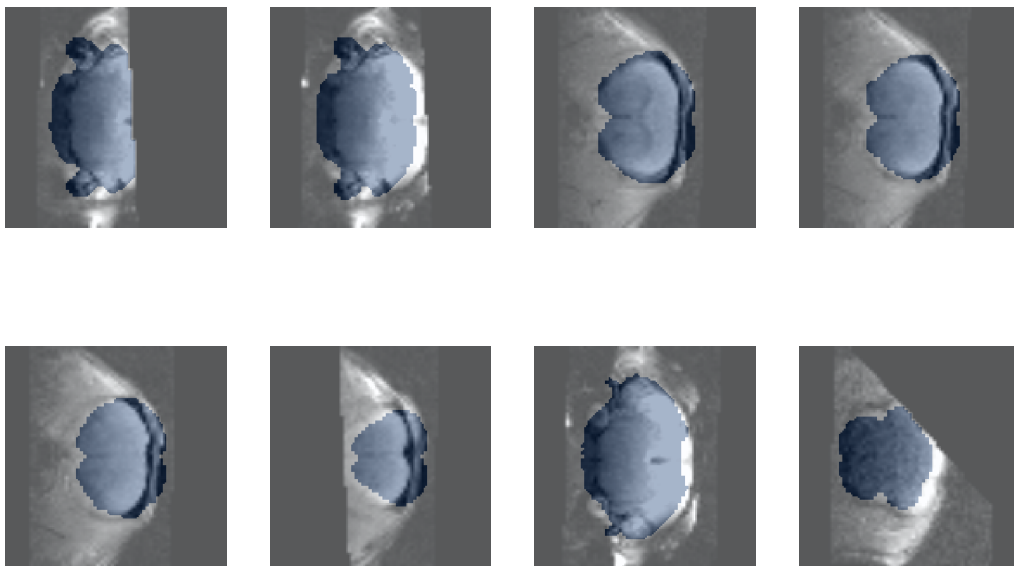


**Figure 6:** Slices where the mask includes too much outer-brain intensities are excluded from the data set. Examples from the slices that were excluded from the data set. The mask is shown in blue, on top of the brain image.

## Supplementary Materials

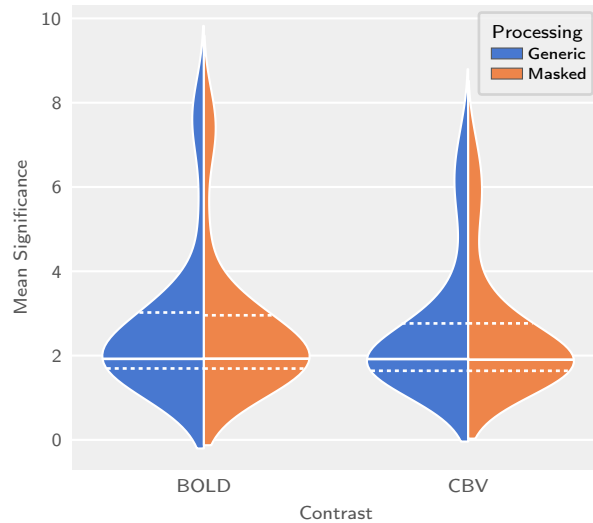


**Figure S1:** The Generic Masked workflow does not introduce a loss of significance. Comparison across workflows and functional contrasts.

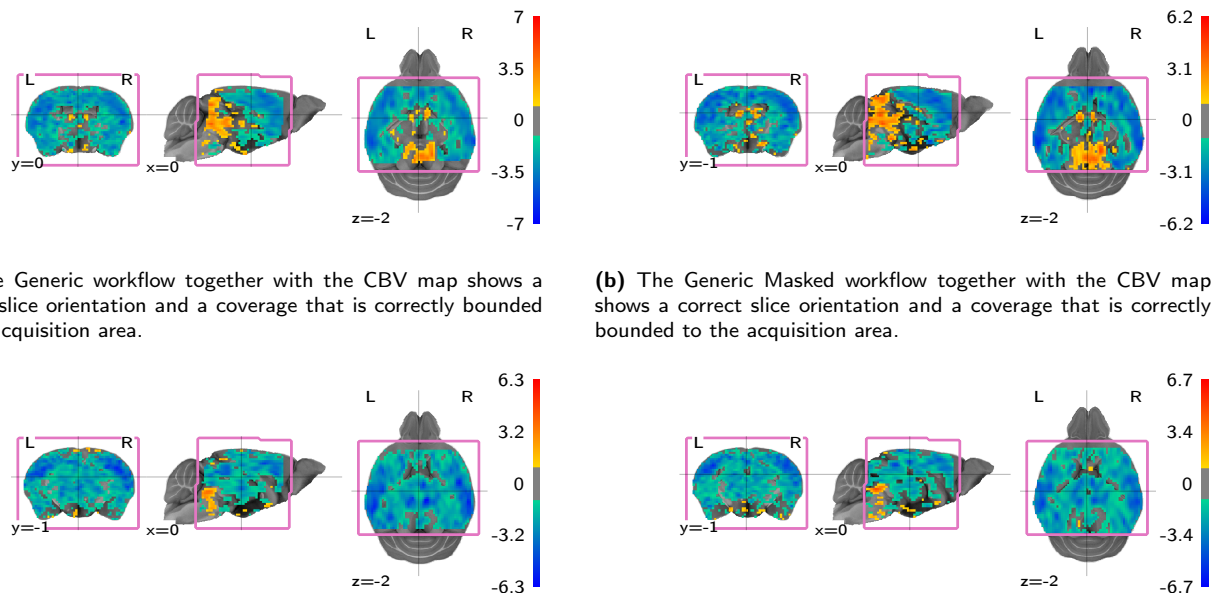
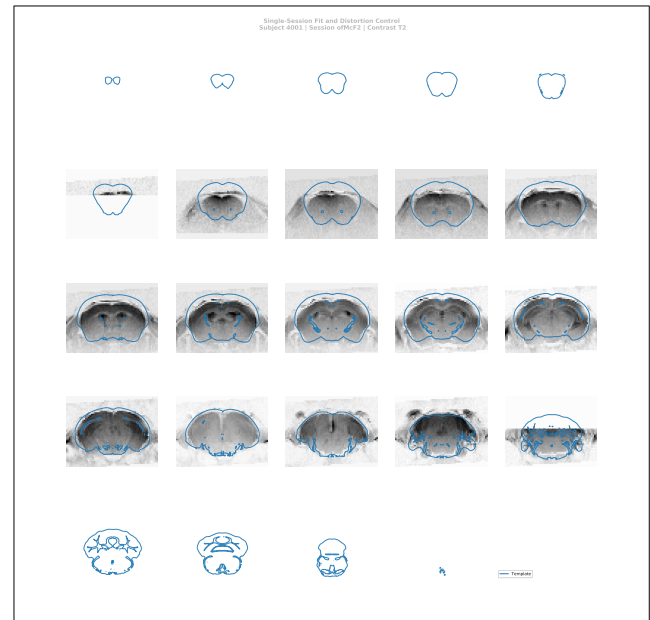


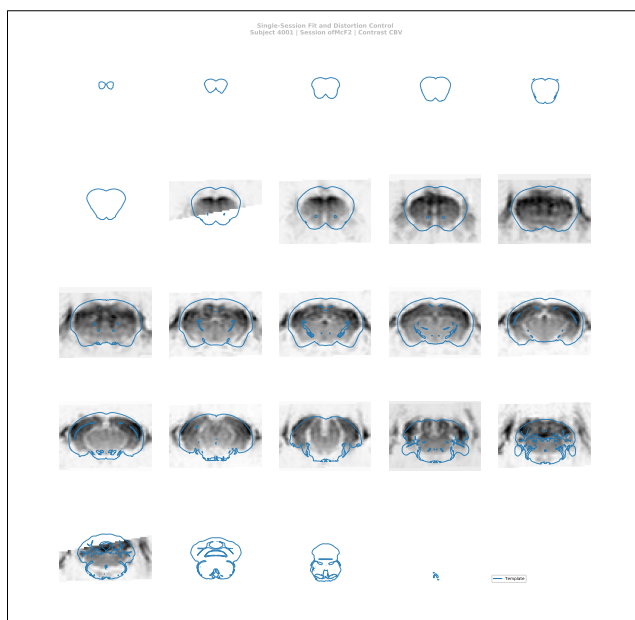
**Figure S2:** The Generic Masked workflow does not induce statistic coverage misalignment nor does it induce overflow of the statistic maps into adjacent anatomical regions. Four multiplanar depictions of second-level omnibus statistic maps thresholded at  $|t| \geq 2$  are shown, corresponding to CBV and BOLD scans. The acquisition area is outlined by the pink square.



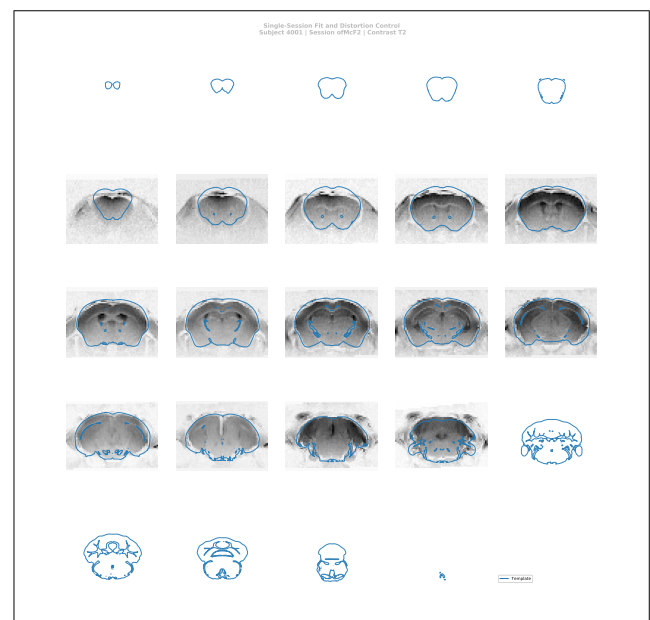
**(a)** SAMRI Generic workflow, depicting an undistorted functional scan intermediary;



**(b)** SAMRI Generic workflow, depicting an undistorted structural scan intermediary;



**(c)** SAMRI Generic Masked workflow, depicting an undistorted functional scan intermediary;



**(d)** SAMRI Generic Masked workflow, depicting an undistorted structural scan intermediary;

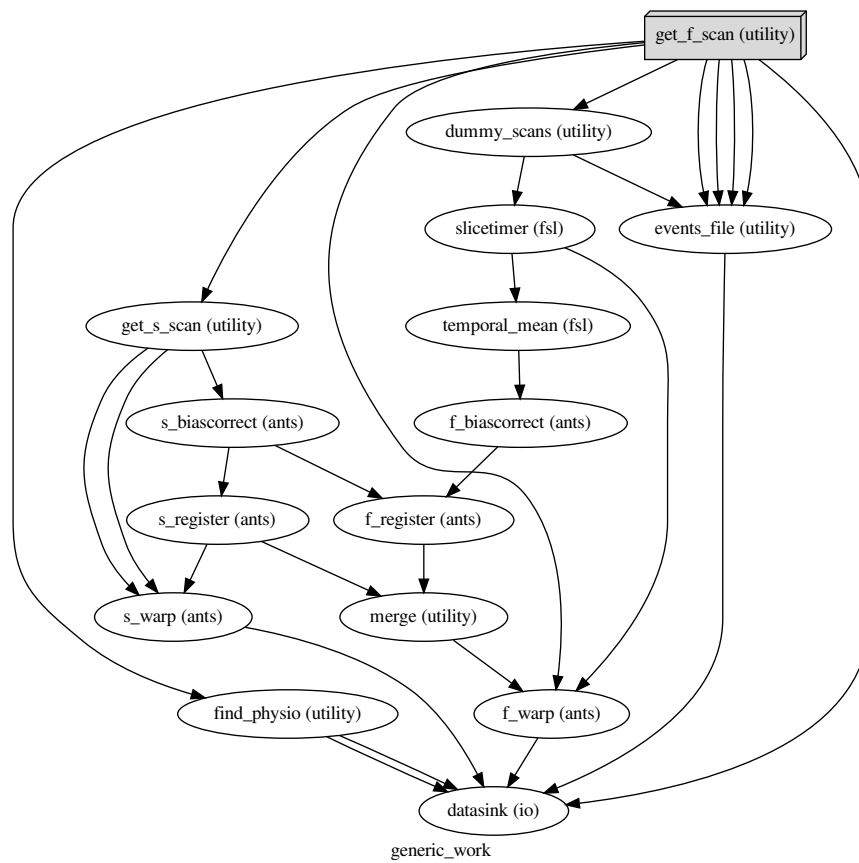
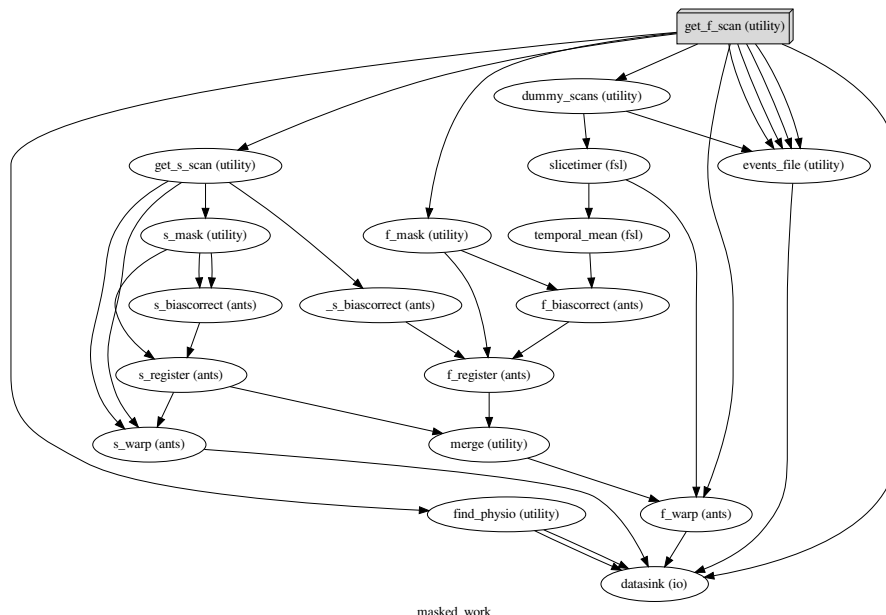
**Figure S3: The SAMRI Generic Masked provides a more accurate coverage of the template space.** Depicted are slice-by-slice inspections of the registration fit, with a spacing that is analogous to acquisition.



(a) A slice-by-slice overview of the SAMRI Generic registration coherence across multiple sessions.



**Figure S4: Both the SAMRI Generic and the Generic Masked workflow present a consistent mapping across sessions.**

(a) "SAMRI Generic" workflow, based on the `antsRegistration` function.(b) "SAMRI Generic Masked" workflow, which is based on the `antsRegistration` function. Two additional nodes provide the workflow with both the masked image and the binary mask.

**Figure S5:** Directed acyclic graphs visualising the two registration workflows. Each node name is depicted together with its corresponding package name in parenthesis. The "utility" indication corresponds to nodes based on Python functions specific to the workflow, distributed alongside it, and dynamically wrapped via Nipype.